Long-term drought severity variations in Morocco

Jan Esper,[1] David Frank,[1] Ulf Büntgen,[1] Anne Verstege,[1] Jürg Luterbacher,[2] and Elena Xoplaki[2]

[1] *Cedrus atlantica* ring width data are used to reconstruct long-term changes in the Palmer Drought Severity Index (PDSI) over the past 953 years in Morocco, NW Africa. The reconstruction captures the dry conditions since the 1980s well and places this extreme period within a millennium-long context. PDSI values were above average for most of the 1450–1980 period, which let recent drought appear exceptional. However, our results also indicate that this pluvial episode of the past millennium was preceded by generally drier conditions back to 1049. Comparison of PDSI estimates with large-scale pressure field reconstructions revealed steady synoptic patterns for drought conditions over the past 350 years. The long-term changes from initially dry to pluvial to recent dry conditions are similar to PDSI trends reported from N America, and we suggest that they are related to long-term temperature changes, potentially teleconnected with ENSO variability and forced by solar irradiance changes. **Citation:** Esper, J., D. Frank, U. Büntgen, A. Verstege, J. Luterbacher, and E. Xoplaki (2007), Long-term drought severity variations in Morocco, *Geophys. Res. Lett.*, *34*, L17702, doi:10.1029/2007GL030844.

1. Introduction

[2] Analysis of the PDSI, a standardized measure of surface moisture conditions [*Palmer*, 1965], revealed distinct 20th century aridity changes in vulnerable NW Africa, including a sharp downward trend towards drier conditions in the 1980s [*Luterbacher et al.*, 2006, and references therein]. While this trend is largely related to changes in precipitation, the persistence of drought until present seems to be forced additionally by regional surface warming [*Dai et al.*, 2004].

[3] Drought of this duration and magnitude has severe socio-ecological consequences. Yet a high-resolution long-term reconstruction that could place current conditions in the context of the past millennium [*Treydte et al.*, 2006; *Cook et al.*, 2004] is missing for N Africa. Such an evaluation of modern drought requires the analysis of proxy data that (i) include updated measurements into the 21st century, (ii) are capable of retaining both high and low frequency variability related to PDSI variation, and (iii) span much of the past millennium.

[4] Analyses of *Cedrus atlantica* ring width data from Morocco indicate sensitivity of these trees to precipitation variation [*Esper et al.*, 2006], the PDSI [*Guiot et al.*, 2005]

and NAO variations [*Glueck and Stockton*, 2001; *Cook et al.*, 2002], and allowed spatial patterns of moisture anomalies over the past 150 years to be derived [*Chbouki et al.*, 1995]. *Till and Guiot* [1990] used cedar trees sampled in the mid 1970s, and reconstructed annual to multi-decadal scale precipitation variation back to the 12th century.

[5] Here we re-use *Cedrus atlantica* tree-ring data generated in the 1980s [*Glueck and Stockton*, 2001] and combine these measurements with a major update collected in 2002. This update allows analysis of tree growth and instrumental data during the current drought episode in comparison to PDSI estimates back to AD 1049. Our study is designed to retain the full spectrum of PDSI variability, from inter-annual to centennial scales. Emphasis is placed on mid-troposphere synoptic modes that trigger extreme dry and wet conditions in Morocco.

2. Material and Methods

2.1. PDSI and Tree-Ring Data

[6] We used monthly 2.5° gridded PDSI data from *Dai et al.* [2004] as the target drought metric, and specified the mean of four highly correlated grid points for proxy calibration (Figure 1). Data were considered back to 1931, as several meteorological stations, including Midelt in the center of the old growth tree sites, started recording precipitation then [*Knippertz et al.*, 2003]. With a lag-1 autocorrelation of about 0.7 over the 1931–2001 period, PDSI persistence is similar to that of cedar tree-rings, suggesting a match between the spectral properties of the predictor and predictand [*Frank and Esper*, 2005].

[7] Tree-ring data used in this study include ~64,000 annual ring width measurements from *Cedrus atlantica* trees sampled in 1985 [*Glueck and Stockton*, 2001], and a newer collection of ~100,000 measurements sampled in 2002. While the original dataset also contains sites with younger (<400 years) trees in the Rif, Middle and High Atlas, the update focused on old growth cedar forests (except for Iso; see auxiliary Table S1[1]). In the 2002 field campaign we sampled all tree age classes to allow for comparisons of signals between differently aged cedars.

[8] Four sites from elevations >2,100 m in the Middle (Tiz and Col) and High Atlas (Tou and Jaf) had cedar trees >500 years. As these sites are within a radius of about 50 km and mean site chronologies share common high to low frequency variance, we merged the old growth sites to a combined dataset TCTJ. TCTJ integrates 326 tree-ring series with a mean length of 412 years. For the purpose of exploring PDSI-related long-term trends and to evaluate potential biases in juvenile tree-rings, we also used subsets

---

[1]Swiss Federal Research Institute for Forest, Snow and Landscape Research, Birmensdorf, Switzerland.

[2]National Centre of Competence in Research on Climate (NCCR) and Institute of Geography, University of Bern, Bern, Switzerland.
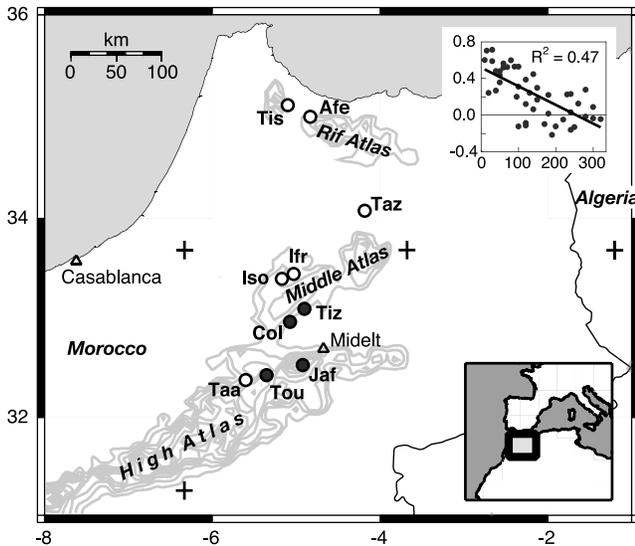
Figure 1. Cedar sampling sites (circles) and PDSI grid points (pluses) in Morocco. Filled circles indicate the old growth (>500 years) tree sites Tiz, Col, Jaf and Tou in the Middle and High Atlas. Scatter plot shows the decay in correlation (y-axis) with increasing distance (x-axis, in kilometer) between sampling sites. Correlations were computed between site chronologies over the 1751–1984 period.

of TCTJ where we excluded trees younger than AD 1600 and even 1400 (see auxiliary material).

2.2. Reconstruction Trials

[9] We applied various detrending techniques to the TCTJ datasets to evaluate long-term trends in resulting chronologies (see auxiliary material). These included Regional Curve Standardization (RCS) [*Esper et al.*, 2003a], Age Banding [*Briffa et al.*, 2001], individual negative exponential detrending [*Fritts*, 1976], and regular normalization [*Esper et al.*, 2003b]. Resulting chronologies are termed RCS, RCS Old, AgeBand, NegExp, and Norm.

[10] For drought reconstruction we spliced the (shorter) Norm and (longer) RCS Old chronology to Norm-RCS (see Figure S6), and regressed this record over the 1931–2001 period against February–June PDSI data [*Dai et al.*, 2004]. For calibration/verification tests we utilized the 1931–1965 and 1966–2001 sub-periods with the R^2, RE, and CE statistics [*Cook et al.*, 1994], and analyzed trend in regression residuals. Three types of error were assigned to estimate reconstruction uncertainty over the past millennium. These include error from (*i*) the difficulty of selecting the most appropriate detrending method (detrending error), (*ii*) the temporally changing number and variance of ring width series combined in a chronology (chronology error), and (*iii*) the unexplained variance in the calibration regression model (calibration error).

[11] For circulation pattern analysis, we used European scale gridded 500 hPa geopotential height data over the 1948–2002 period [*Kistler et al.*, 2001] and reconstructed fields at monthly resolution back to 1659 [*Luterbacher et al.*, 2002]. A scaled composite analysis [*Brown and Hall*, 1999] was applied to extract the relevant mid-troposphere pressure patterns triggering extreme PDSI anomalies, i.e., years that exceed 1.5 standard deviations from the long-term mean. Circulation pattern detection was applied over the full 1659–2001 period, and the 1948–2001 and pre-1900 sub-periods.

3. Results

3.1. PDSI History

[12] The long-term PDSI reconstruction indicates generally drier conditions before ~1350, a transition period until ~1450, and generally wetter conditions until the 1970s (Figure 2). Superimposed on this long-term behavior are distinct decadal scale fluctuations including current drought since the early 1980s. While the driest 20-year period reconstructed is 1237–1256 (PDSI = −4.2), 1981–2000 conditions are in line with this historical extreme (−3.9).

[13] Calibration/verification tests of the linear regressed Norm-RCS data indicated skill of the model in the high-to-low frequency domains. R^2 ranged 0.43–0.58, and RE
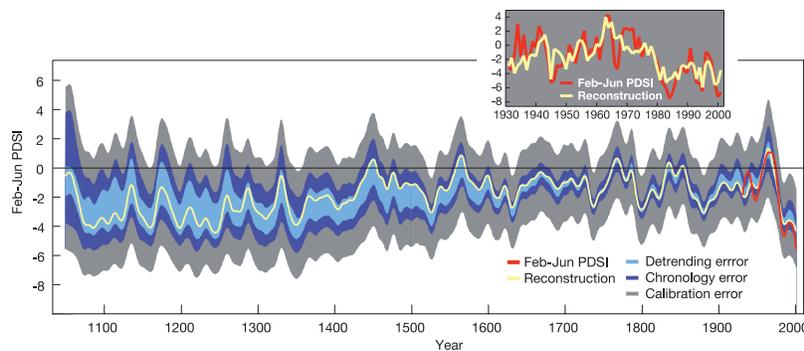
Figure 2. February–June PDSI reconstruction (yellow curve) back to 1049. Bands around the reconstruction specify various error terms, including the upper and lower bounds of five differently detrended chronologies (light blue, detrending error), 95% bootstrap confidence intervals (dark blue, chronology error), and the two standard error confidence range from the regression model (gray, calibration error). Red curve is the instrumental PDSI data. Insert table shows the (unsmoothed) reconstruction and target timeseries for the 1931–2001 period of overlap. Zero line refers to the global instrumental PDSI dataset derived from *Dai et al.* [2004]. All series smoothed with a 20-year filter.
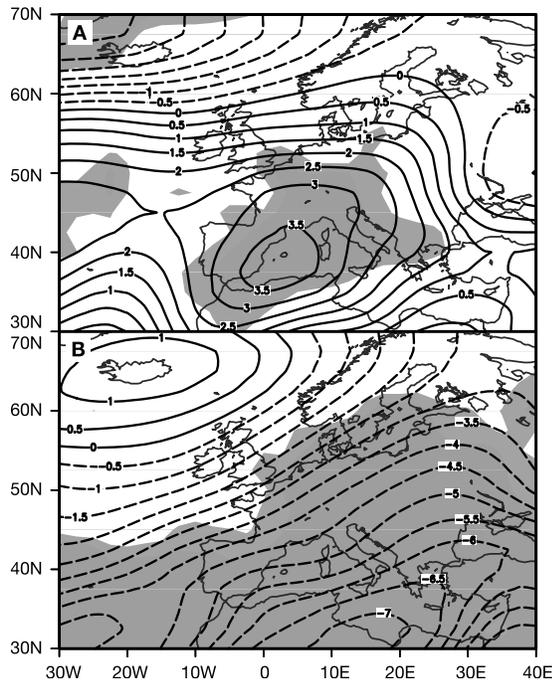
Figure 3. Scaled anomaly composites of the February–June 500 hPa patterns for the (a) 15 driest and (b) 32 wettest years reconstructed over 1659–2001 in Morocco. 90% significant areas are highlighted in gray. Units are arbitrary.

and CE 0.63–0.67 and 0.35–0.50, respectively (see Table S2). When calibrated over the full 1931–2001 period, the model explains 56% of February–June PDSI variability, and analysis of the regression revealed little trend in model residuals. The February–June seasonality is, however, not very distinct, as monthly PDSI series are highly correlated. Similarly good results were thus obtained when including cold season months (e.g., October–June). Importantly, the change from wet conditions until the 1970s to subsequently dry conditions is fully retained in the proxy data. Most of the reconstructed, pre-instrumental variance is captured in the 1931–2001 calibration period, both suggesting a robust calibration as little extrapolation outside the calibration interval occurs and emphasizing the extreme nature of the recent moisture fluctuations.

[14] While the (conservatively) stacked errors (Figure 2) indicate some decadal scale droughts (e.g., ca. 1800s, 1880s, 1980/90s, and earlier in the last millennium ca. 1350s and 1520s) deviate significantly from the instrumental mean, confidence of the long-term trends remains lower. This assessment reflects both the greater uncertainty in low-frequency variation from detrending, and how the individual errors are combined. For comparison, see Figure S7 for the narrower uncertainty bands derived from root-summed-squared errors.

3.2. Regional to Large-Scale Comparison

[15] Analysis of extreme February-June PDSI values reconstructed since 1659–the period from which monthly 500 hPa pressure fields are available [*Luterbacher et al.*, 2002]–showed that very dry years cohere with positive geopotential height anomalies stretching from NW Africa to central Europe (Figure 3). This pattern is indicative of a strong Azores high, a northerly shift of North Atlantic cyclones, and reduced westerly humidity advection into Morocco. On the contrary, very wet years cohere with anomalous negative mid-troposphere pressure variations over Mediterranean and parts of central Europe. Pluvial conditions are driven by increased frequencies of westerly circulation regimes transporting moist and mild air from the subtropical Atlantic onto the northwestern edge of the African continent. Further assessment of extreme PDSI deviations, utilizing a split-period instrumental versus pre-instrumental approach (see the auxiliary material), indicated only slight shifts in pressure center position and intensity over the past 350 years.

[16] Comparison of the new PDSI record with long-term aridity changes reconstructed in the United States [*Cook et al.*, 2004] indicated similarity in the low frequency, centennial scale behavior (Figure 4). Albeit the error bars of such timeseries generally increase back in time, both the US and Moroccan records indicate a changed Medieval hydroclimate characterized by drier conditions until about the 15th century. Also the pluvial second half of the millennium and the recent drying trend are quite similar between these regions from where long-term PDSI reconstructions are available. Moreover, association with millennium-long temperature reconstructions from Europe [*Büntgen et al.*, 2006] and the Northern Hemisphere (not shown) [*Esper et al.*, 2002] indicate that Moroccan drought changes are broadly coherent with well-documented temperature fluctuations including warmth during medieval times, cold in the Little Ice Age (LIA), and recent anthropogenic warming (Figure 4c).

4. Discussion

[17] Analyses of global PDSI data revealed sustained drought in the late 20th century in N Africa with contributions from both decreased precipitation and increased temperatures [*Dai et al.*, 2004]. This drought is also expressed in a progressive expansion of the Sahara as seen in satellite-derived vegetation index data [*Tucker et al.*, 1991]. Drought in the Atlas mountains of Morocco is correlated with the strength and position of the Azores high and associated northward shifts of North Atlantic storm tracks during winter and spring. While these synoptic patterns are well understood for the instrumental period [*Knippertz et al.*, 2003; *Xoplaki et al.*, 2004], the combination of drought and pressure field reconstructions as presented here, allows assessment of the relevant circulation patterns over longer timescales. Results indicate that the mid-troposphere pressure patterns related to regionally dry and wet conditions were rather stable at least back to the mid seventeenth century.

[18] To this end, we detailed evidence that the late 20th century drought is exceptional in context of the past 500 years, but appears more typical when associated with conditions before 1400. Similarly extreme and persistent medieval drought has been reconstructed via lake-level and salinity variations in equatorial E Africa [*Verschuren et al.*, 2000] and the Sierra Nevada, California [*Stine*, 1994], for example. Various palaeoclimatic records, including a seminal PDSI reconstruction from a large N American tree-ring
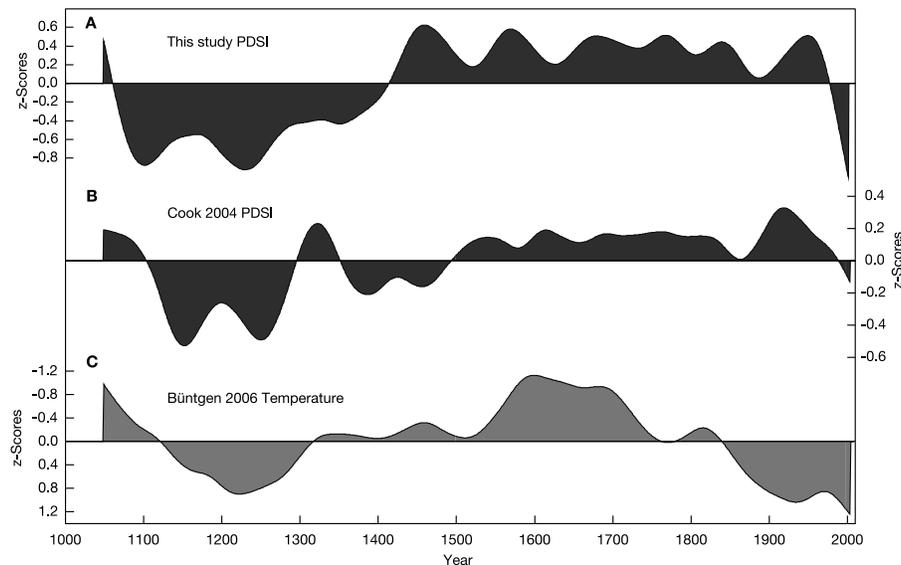
Figure 4. Comparison of the long-term PDSI reconstruction (a) from Morocco, (b) with the PDSI-based drought area index from the western United States, and with (c) the (inverted) temperature record from the European Alps. All data normalized and smoothed using a 120-year spline filter.

network [*Cook et al.*, 2004], indicate reduced surface moistening and pronounced increases in drought frequency during medieval times in several places of the subtropics [*Herweijer et al.*, 2006].

[19] The persistent medieval dry conditions and successive LIA moistening reported here, were probably forced by North Atlantic sea surface temperature (SST) and associated thermohaline circulation (THC) changes [*Scourse et al.*, 2006]. Recent shallow marine palaeoceanographic studies revealed substantial reorganizations of the ocean-climate system including warmer SSTs and active THC early in the last millennium, followed by much colder SST and reduced THC after 1300 until about 1900 [*Hebbeln et al.*, 2006]. These notable changes recorded in marine localities on the W European shelf are consistent with surface temperature reconstructions from the European continent [*Büntgen et al.*, 2006] and were potentially coupled via the NAO with Moroccan surface droughts.

[20] Association of a strengthened THC with a poleward shift of westerly storm tracks was recently suggested [*Seager et al.*, 2007] to be teleconnected with persistent La Niña-like conditions in the tropical Pacific [*Cobb et al.*, 2003], the major driver for medieval drought in N America [*Cook et al.*, 2007; *Graham et al.*, 2007]. Similar considerations might also account for the persistently drier conditions now reconstructed for NW Africa. The long-term change towards pluvial LIA conditions has been assessed using coupled ocean-atmosphere climate models forced by multi-decadal solar irradiance increases [*Shindell et al.*, 2006]. Such simulations indicate that greater tropical temperatures–due to increased solar irradiance and similarly but less significantly due to increased greenhouse gases– fundamentally alter the hydrological cycle. Consequences of these hydrological shifts include increased precipitation along the equator and a general drying of the subtropics, a pattern now supported by this study. The ultimate drivers

for this medieval hydroclimate pattern seemed to be high solar irradiance and low volcanic forcings [*Emile-Geay et al.*, 2007].

References

Briffa, K. R., T. J. Osborn, F. H. Schweingruber, I. C. Harris, P. D. Jones, S. G. Shiyatov, and E. A. Vaganov (2001), Low-frequency temperature variations from a northern tree ring density network, *J. Geophys. Res.*, *106*, 2929–2941.

Brown, T. J., and B. L. Hall (1999), The use of *t*-values in climatological composite analyses, *J. Clim.*, *12*, 2941–2944.

Büntgen, U., D. C. Frank, D. Nievergelt, and J. Esper (2006), Alpine summer temperature variations AD 755–2004, *J. Clim.*, *19*, 5606–5623.

Chbouki, N., C. W. Stockton, and D. M. Myers (1995), Spatio-temporal patterns of drought in Morocco, *Int. J. Climatol.*, *15*, 187–205.

Cobb, K. M., C. D. Charles, H. Cheng, and R. L. Edwards (2003), El Niño/ Southern Oscillation and tropical Pacific climate change during the last millennium, *Nature*, *424*, 271–276.

Cook, E. R., K. R. Briffa, and P. D. Jones (1994), Spatial regression methods in dendroclimatology: A review and comparison of two techniques, *Int. J. Climatol.*, *14*, 379–402.

Cook, E. R., R. D. D'Arrigo, and M. E. Mann (2002), A well-verified multiproxy reconstruction of the winter North Atlantic Oscillation index since A. D. 1400, *J. Clim.*, *15*, 1754–1764.

Cook, E. R., C. A. Woodhouse, C. M. Eakin, D. M. Meko, and D. W. Stahle (2004), Long-term aridity changes in the western United States, *Science*, *306*, 1015–1018.

Cook, E. R., R. Seager, M. A. Cane, and D. W. Stahle (2007), North American drought: Reconstructions, causes and consequences, *Quat. Sci. Rev.*, *81*, 93–134.

Dai, A., K. E. Trenberth, and T. Qian (2004), A global dataset of Palmer drought severity index for 1870–2002: Relationship with soil moisture and effects of surface warming, *J. Hydrometeorol.*, *5*, 1117–1130.

Emile-Geay, J., M. Cane, R. Seager, A. Kaplan, and P. Almasi (2007), El Niño as a mediator of the solar influence on climate, *Paleoceanography*, *22*, PA3210, doi:10.1029/2006PA001304.

Esper, J., E. R. Cook, and F. H. Schweingruber (2002), Low-frequency signals in long tree-ring chronologies for reconstructing past temperature variability, *Science*, *295*, 2250–2253.

Esper, J., E. R. Cook, P. J. Krusic, K. Peters, and F. H. Schweingruber (2003a), Tests of the RCS method for preserving low-frequency variability in long tree-ring chronologies, *Tree Ring Res.*, *59*, 81–98.

Esper, J., S. G. Shiyatov, V. S. Mazepa, R. J. S. Wilson, D. A. Graybill, and G. Funkhouser (2003b), Temperature-sensitive Tien Shan tree ring chronologies show multi-centennial growth trends, *Clim. Dyn.*, *8*, 699–706.

Esper, J., U. Büntgen, D. C. Frank, D. Nievergelt, K. Treydte, and A. Verstege (2006), Multiple tree-ring parameters from Atlas cedar (Morocco) and their climatic signal, in *Tree Rings in Archaeology, Climatology and Ecology, Reihe Umwelt Environ.*, vol. 61, edited by I. Heinrich et al., pp. 46–55, Forschungszentrum Jülich, Jülich, Germany.

Frank, D., and J. Esper (2005), Temperature reconstructions and comparisons with instrumental data from a tree-ring network for the European Alps, *Int. J. Climatol.*, *25*, 1437–1454.

Fritts, H. C. (1976), *Tree Rings and Climate*, 567 pp., Academic, London.

Glueck, M. F., and C. W. Stockton (2001), Reconstruction of the North Atlantic Oscillation, 1429–1983, *Int. J. Climatol.*, *21*, 1453–1465.

Graham, N. E., et al. (2007), Tropical Pacific mid-latitude teleconnections in medieval times, *Clim. Change*, *83*, 241–285.

Guiot, J., S. Alleaume, A. Nicault, and S. Brewer (2005), The Mediterranean droughts during the last 650 years: Reconstruction from tree-rings and climate model simulation, *Geophys. Res. Abstracts*, *7*, 02471.

Hebbeln, D., et al. (2006), Late Holocene coastal hydrographic and climate changes in the eastern North Sea, *Holocene*, *16*, 987–1001.

Herweijer, C., R. Seager, and E. R. Cook (2006), North American droughts of the mid to late nineteenth century: A history, simulation and implication for mediaeval drought, *Holocene*, *16*, 159–171.

Kistler, R., et al. (2001), The NCEP-NCAR 50-year reanalysis: Monthly means CD-ROM and documentation, *Bull. Am. Meteorol. Soc.*, *82*, 247–267.

Knippertz, P., M. Christoph, and P. Speth (2003), Long-term precipitation variability in Morocco and the link to the large-scale circulation in recent and future climates, *Meteorol. Atmos. Phys.*, *83*, 67–88.

Luterbacher, J., E. Xoplaki, D. Dietrich, R. Rickli, J. Jacobeit, C. Beck, D. Gyalistras, C. Schmutz, and H. Wanner (2002), Reconstruction of sea-level pressure fields over the eastern North Atlantic and Europe back to 1500, *Clim. Dyn.*, *18*, 545–561.

Luterbacher, J., et al. (2006), Mediterranean climate variability over the last centuries: A review, in *The Mediterranean Climate*, edited by P. Lionello et al., pp. 27–148, Elsevier, Amsterdam.

Palmer, W. C. (1965), Meteorological drought, *Res. Pap. 45*, 58 pp., U. S. Dep. of Commer., Washington, D. C.

Scourse, J., H. P. Sejrup, and P. D. Jones (2006), Late Holocene oceanographic and climate change from the western European margin: The results of the Holsmeer project, *Holocene*, *16*, 931–935.

Seager, R., N. Graham, C. Herweijer, A. L. Gordon, Y. Kushnir, and E. Cook (2007), Blueprints for medieval hydroclimate, *Quat. Sci. Rev.*, in press.

Shindell, D. T., G. Faluvegi, R. L. Miller, G. A. Schmidt, J. E. Hansen, and S. Sun (2006), Solar and anthropogenic forcing of tropical hydrology, *Geophys. Res. Lett.*, *33*, L24706, doi:10.1029/2006GL027468.

Stine, S. (1994), Extreme and persistent drought in California and Patagonia during mediaeval time, *Nature*, *369*, 546–549.

Till, C., and J. Guiot (1990), Reconstruction of precipitation in Morocco since 1100 A. D. based on Cedrus atlantica tree-ring widths, *Quat. Res.*, *33*, 337–351.

Treydte, K., G. H. Schleser, G. Helle, D. C. Frank, M. Winiger, G. H. Haug, and J. Esper (2006), Millennium-long precipitation record from tree-ring oxygen isotopes in northern Pakistan, *Nature*, *440*, 1179–1182.

Tucker, C. J., H. E. Dregne, and W. W. Newcomb (1991), Expansion and contraction of the Sahara Desert from 1980 to 1990, *Science*, *253*, 299–301.

Verschuren, D., K. R. Laird, and B. F. Cumming (2000), Rainfall and drought in equatorial East Africa during the past 1100 years, *Nature*, *403*, 410–414.

Xoplaki, E., J. F. Gonzalez-Rouco, J. Luterbacher, and H. Wanner (2004), Wet season Mediterranean precipitation variability: Influence of large-scale dynamics and trends, *Clim. Dyn.*, *23*, 63–78.

———————————

U. Büntgen, J. Esper, D. Frank, and A. Verstege, Swiss Federal Research Institute for Forest, Snow and Landscape Research, CH-8903 Birmensdorf, Switzerland. (esper@wsl.ch)

J. Luterbacher and E. Xoplaki, National Centre of Competence in Research on Climate (NCCR) and Institute of Geography, University of Bern, CH-3012 Bern, Switzerland.